Electronic Supporting Information (ESI)

Nanostructured $DyFeO_3$ Photocatalyst: An Authentic and Effective Approach for Remediation of Industrial and Pharmaceutical Wastewater

Mohasin Tarek, Ferdous Yasmeen, M. A. Basith

Nanotechnology Research Laboratory, Department of Physics,

Bangladesh University of Engineering and Technology, Dhaka-1000, Bangladesh..

*Corresponding author(s). E-mail: mabasith@phy.buet.ac.bd

Sample preparation

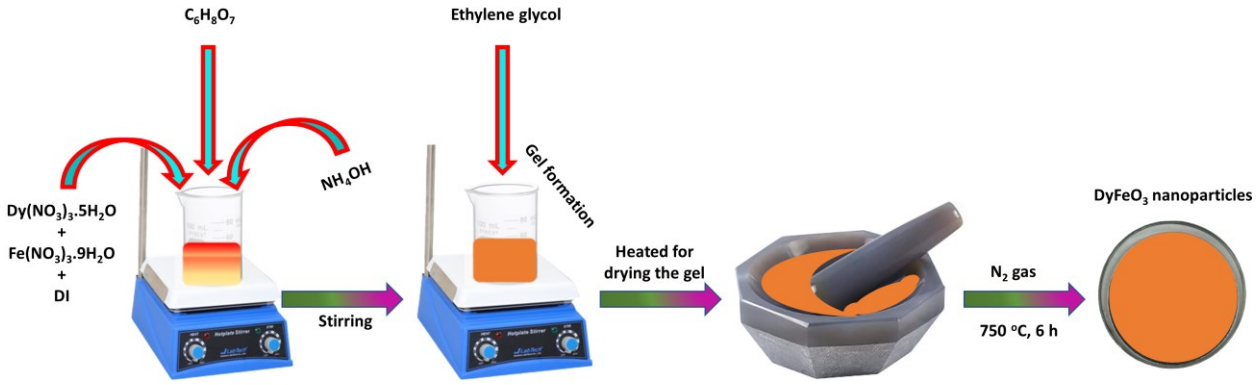

Fig. S1. *Schematic representation of the synthesis procedure of porous $DyFeO_3$ nanoparticles by sol-gel technique.*

Nanoparticles of $DyFeO_3$ perovskite were synthesized using a sol-gel method, as illustrated in Figure S1 [1]. Initially, precise stoichiometric amounts of $Dy(NO_3)_3 \cdot 5H_2O$ and $Fe(NO_3)_3 \cdot 9H_2O$ were each dissolved separately in 100 ml of deionized water and stirred for 15-20 minutes using a magnetic stirrer to ensure complete dissolution. The individual solutions were then combined, and

citric acid ($C_6H_8O_7$) was added to the mixture. Citric acid acts as a chelating agent, binding to the metal ions to form stable complexes and preventing premature precipitation. The pH of the combined solution was carefully adjusted to 7 by adding ammonium hydroxide (NH_4OH dropwise, ensuring a neutral environment optimal for the subsequent reactions. Following this, ethylene glycol was introduced to the solution. Ethylene glycol serves a dual purpose: it not only acts as a solvent but also facilitates the formation of a polymeric network of metal cations, which is essential for creating the gel precursor. After allowing the mixture to react for four hours at room temperature, the temperature was gradually increased to 200 °C. This increase in temperature initiated the combustion process, where the organic components of the gel decomposed, releasing gases and leaving behind the desired metal oxides in powder form. The combustion was carefully controlled to ensure complete removal of organic residues. The resulting powder was then finely ground using an agate mortar to achieve a uniform particle size. To further enhance the crystallinity and develop the porous structure of the $DyFeO_3$ nanoparticles, the material underwent calcination. This was performed at 750 °C for 6 hours with a precise heating rate of 5 °C per minute in a nitrogen environment. The slow and controlled heating rate minimized thermal stress on the material, preventing cracks and ensuring a uniform structure. The use of nitrogen gas during the calcination process was crucial. It provided an inert atmosphere that prevented unwanted oxidation reactions and controlled the evolution of gases released during decomposition. This controlled atmosphere was essential for achieving the desired porosity and structural properties of the $DyFeO_3$ nanoparticles. The reproducible formation of porous $DyFeO_3$ nanoparticles was meticulously achieved through careful selection of the solvent (deionized water), systematic adjustment of the gel precursor concentration (ethylene glycol), precise control of the reaction and calcination temperatures, and optimization of the nitrogen flow during the calcination process. These steps ensured consistent quality and performance of the synthesized $DyFeO_3$ nanoparticles.

Calculation of yield percentage of $DyFeO_3$ nanoparticles

Step 1: Calculate the theoretical yield

Thus, the molar mass of

$DyFeO_3 = 266.343\ g\ mol^{-1}$

$Dy(NO_3)_3.5H_2O$ = 438.52 g mol^{-1}

$Fe(NO_3)_3.9H_2O$ = 404 g mol^{-1}

Weight of reactants taken during synthesis:

$Dy(NO_3)_3.5H_2O$ = 4.9393 g

$Fe(NO_3)_3.9H_2O$ = 4.5505 g

Moles of each reactant:

$Dy(NO_3)_3.5H_2O$ = 4.9393/438.52 = 0.011263568 mol

$Fe(NO_3)_3.9H_2O$ = 4.5505/404 = 0.011263568 mol

Limiting Reactant:

Since the molar ratio of Dy to Fe in $DyFeO_3$ nanoparticles is 1:1, the moles of $Dy(NO_3)_3.5H_2O$ and $Fe(NO_3)_3.9H_2O$ are equal. We can use either to find the theoretical yield.

Theoretical yield of $DyFeO_3$ nanoparticles:

Theoretical yield = 0.011263568 mol × 266.343 g/mol = 2.999 g

Step 2: Actual yield of $DyFeO_3$ nanoparticles

After synthesis, we obtained approximately 2.85 g of $DyFeO_3$ nanoparticles

$$\text{Actual yield percentage of } DyFeO_3 = \frac{\text{Actual yield}}{\text{Theoretical yield}} \times 100\% = \frac{2.85}{2.999} \times 100\% = 95\%$$

Electrochemical cell setup for Mott-Schottky analysis

A three-electrode system was employed utilizing a 0.5 M Na_2SO_4 aqueous solution as the electrolyte. In this configuration, an Ag/AgCl electrode immersed in a saturated 3.5 M KCl solution served as the reference electrode, while a platinum wire functioned as the counter electrode. To fabricate the working electrode, 20 mg of the synthesized $DyFeO_3$ nanoparticles (constituting 90 wt%) was mixed with 2.22 mg of polyvinylidene fluoride (PVDF; 10 wt%) serving

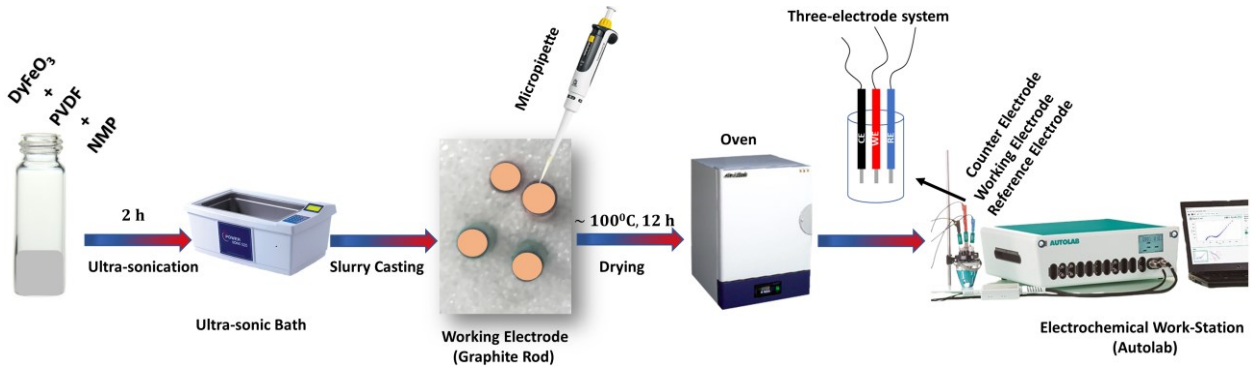

Fig. S2 *Schematic illustration of the preparation of electrode slurry and the configuration of the electrochemical setup.*

as a binder, and 200 µL of N-methyl-2-pyrrolidone (NMP) as a solvent. This mixture was sonicated for 2 hours to achieve a homogeneous slurry. The resultant slurry was then uniformly cast onto a graphite rod with a surface area of 0.28 cm^2. The coated graphite rod was subsequently dried at

100°C for 12 hours to ensure complete solvent evaporation and proper adhesion of the active material. This modified graphite rod was subsequently used as the working electrode for Mott-Schottky analysis.

Experimental setup for photocatalytic degradation of pollutants from water

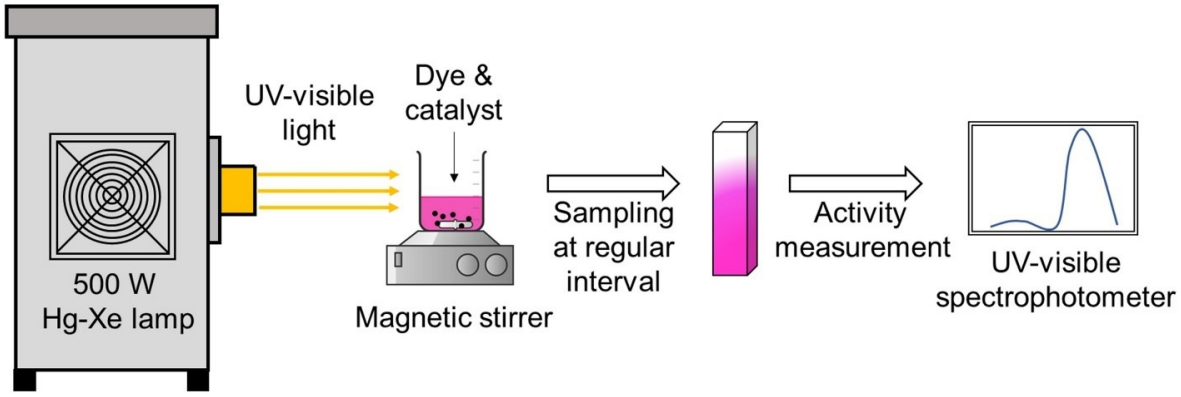

Fig. S3. *Schematically a photocatalytic reactor setup for the pollutant degradation experiments. Irradiation power density was 100 mW cm^{-2}.*

Table S1 Crystallographic *parameters of the as-synthesized porous $DyFeO_3$ nanoparticles before and after 4 cycles of photocatalysis obtained after Rietveld refinement. Analysis of the XRD data suggests that this material maintained its structural integrity without undergoing any phase transformation making our synthesized nanoparticles a reliable catalyst for photocatalytic wastewater treatment.*

Parameters	Before 4 cycles of photocatalysis	After 4 cycles of photocatalysis
Crystallographic phase	Orthorhombic	Orthorhombic
Space group	*Pnma*	*Pnma*
a (Å)	5.59324	5.59350
b (Å)	7.62289	7.6270
c (Å)	5.30227	5.30235
$\alpha = \beta = \gamma$ (degree)	90	90
Crystallinity (%)	93.47	87.2
Goodness of fit χ^2	2.1	2.3

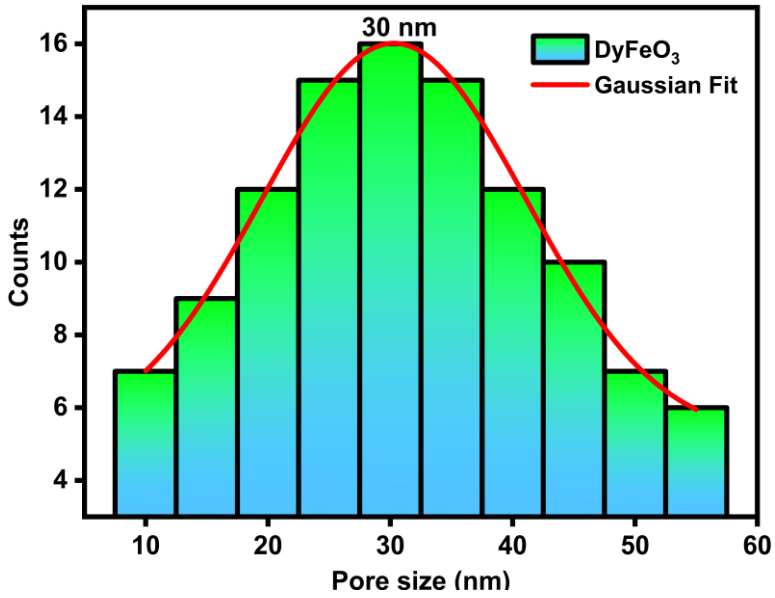

Fig. S4 *The pore size distribution histogram shows that the $DyFeO_3$ sample has nano-sized pores with an average size of 30 nm.*

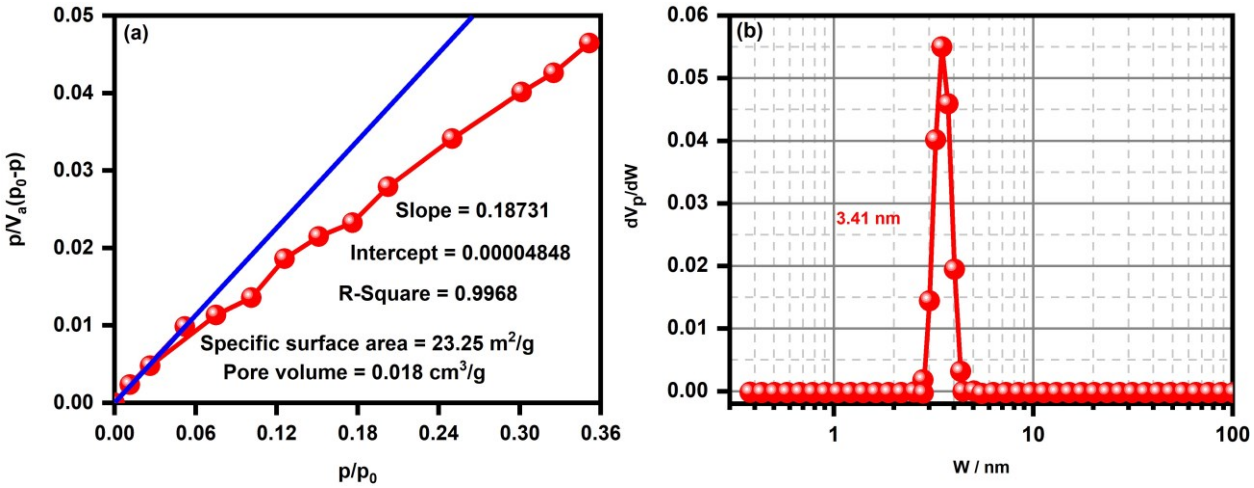

Fig. S5 *Surface area and pore size distribution of porous $DyFeO_3$ nanoparticles by BET analysis. (a) BET plot of porous $DyFeO_3$ nanoparticles based on N_2 adsorption-desorption isotherms. The analysis indicates a specific surface area of 23.25 m^2/g and a pore volume of 0.018 cm^3 g^{-1}, essential for optimizing photocatalytic activity; (b) Pore size distribution of the $DyFeO_3$ nanoparticles calculated using the Non-Local Density Functional Theory (NLDFT) method, showing a sharp peak at 3.41 nm, confirming the mesoporous nature of the material.*

The Brunauer–Emmett–Teller (BET) technique is employed to analyze the specific surface area of $DyFeO_3$ nanoparticles by measuring nitrogen gas adsorption. The BET equation [2]:

$$\frac{p}{V_a(p_0 - p)} = \frac{1}{V_m C} + \frac{C - 1}{V_m C} \times \frac{p}{p_0}$$

relates the relative pressure $\frac{p}{p_0}$ to the volume of gas adsorbed $V_{a,}$ where V_m is the monolayer capacity, and C is the BET constant. By plotting $\frac{p}{V_a(p_0 - p)}$ against $\frac{p}{p_0}$, the slope and intercept of the resulting linear plot allow for the calculation of V_m as:

$$V_m = \frac{1}{Slope + Intercept}$$

The specific surface area is then calculated using the Equation:

$$A = \frac{V_m \times N \times S}{V}$$

Where N is the Avogadro's number (6.023×10^{23} molecules/mol), S is the adsorption cross-section area of the adsorbing species (0.162 nm^2 for N^2) and V is the molar volume of the gas (22.414 L for an ideal gas at STP).

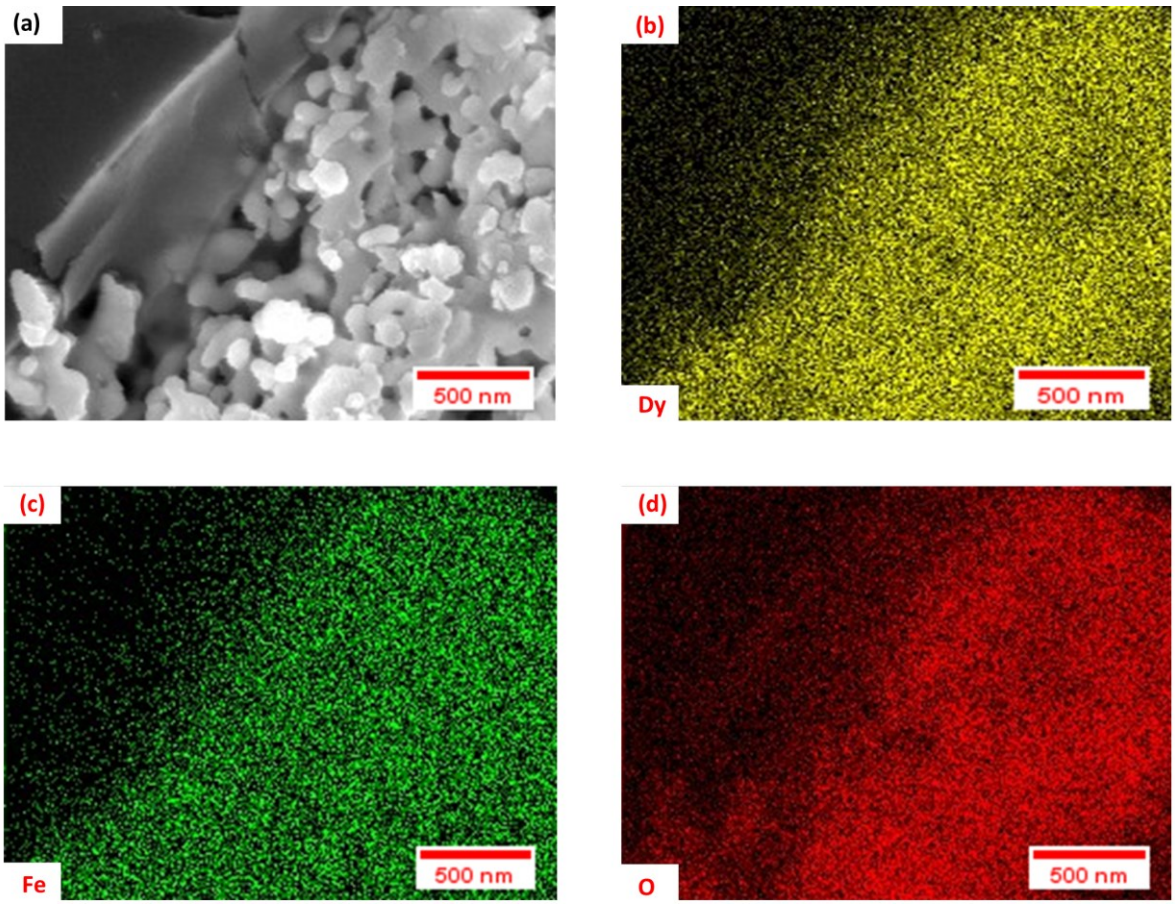

Fig. S6 *The FESEM image in (a) highlights an area where the nanoparticles are partially distributed, allowing for the differentiation between the $DyFeO_3$ particles and the underlying carbon substrate. The elemental mapping images reveal the distribution of each element within the nanoparticles, demonstrating a uniform presence of (b) Dy, (c) Fe, and (d) O in the right-hand region, while the left-hand region shows a darker contrast corresponding to the substrate. This variation in intensity across the mapping images accurately reflects the localized presence of $DyFeO_3$ nanoparticles, providing a clear visual distinction between regions with and without the target material.*

Table S2 *Mass and atomic percentages of corresponding elements in $DyFeO_3$ nanoparticles as obtained via EDX analysis were consistent with theoretical analysis, which indicates the successful formation of $DyFeO_3$ nanoparticles.*

Elements	Mass (%) (theoretical)	Mass (%) (experimental)	Atom (%) (theoretical)	Atom (%) (experimental)
Dy	58.33	60.97	20	17.11
Fe	23.62	22.42	20	23.05
O	17.06	16.61	60	59.84

Table S3 *The XPS spectrum of $DyFeO_3$ nanoparticles before and after 4 cycles of photocatalysis revealed several distinct peaks corresponding to the oxidation states of Dy, Fe and O.*

Element	Orbital	Peaks	Binding energy (eV) (Before photocatalysis)	Binding energy (eV) (After 4 cycles of photocatalysis)
Dy	Dy 3d	$3d_{5/2}$ (Dy^{3+})	1334.61	1334.61
		$3d_{3/2}$ (Dy^{3+})	1296.32	1296.32
Fe	Fe 2p	satellite	733.27	733.27
		$2p_{3/2}$ (Fe^{2+})	725.89	725.89
		$2p_{3/2}$ (Fe^{3+})	724.04	724.04
		satellite	718.91	718.91
		$2p_{1/2}$ (Fe^{2+})	712.5	712.5
		$2p_{1/2}$ (Fe^{3+})	710.52	710.52
O	O 1s	O_{OH^-}	532.29	532.29
		$O_{vcan.}$	530.5	530.5
		O^{2-} (metal oxide)	529.46	529.46

Table S4 *A brief review of the pollutant degrading capabilities exhibited by $DyFeO_3$ nanoparticles photocatalysts compared to other commonly used photocatalysts in recent investigations. This table suggests that our synthesized $DyFeO_3$ nanoparticles photocatalyst exhibited superior photocatalytic degradation performances on both industrial dye and pharmaceutical antibiotics surpassing or comparable with the other photocatalysts.*

Perovskite	Light source	Synthesis method	Pollutant	Pollutant conc.	Catalyst conc.	Irradiation time (min.)	Degradation (%)	Ref.
$BiFeO_3$	500 W Hg-Xe	Sol-gel	Ciprofloxacin	10 mg/L	0.8 g/L	240	42	[3]
$BiFeO_3$	500 W Hg-Xe	Solgel	Levofloxacin	10 mg/L	0.8 g/L	240	46	[3]
$SmFeO_3$	300 W	Sol-gel	Rhodamine B	20 mg/L	1.5 g/ L	300	45	[4]
$LaFeO_3$	200 W Xe	Sol-gel	Rhodamine B	5 mg/L	1 g/L	180	67.4	[5]
$SrFeO_3$	150 W Xe	Combustion	Rhodamine B	5 mg/L	0.3 g/L		43	[6]
$BiFeO_3$	-	Sol-gel	Ciprofloxacin	10 mg/ L	2 g/L	60	<20	[7]
$DyFeO_3$	500 W Hg-Xe	Sol-gel	Rhodamine B	12 mg/L	0.8 g/L	240	85.9	This work
$DyFeO_3$	500 W Hg-Xe	Sol-gel	Levofloxacin	10 mg/L	0.4 g/L	240	88.38	This work

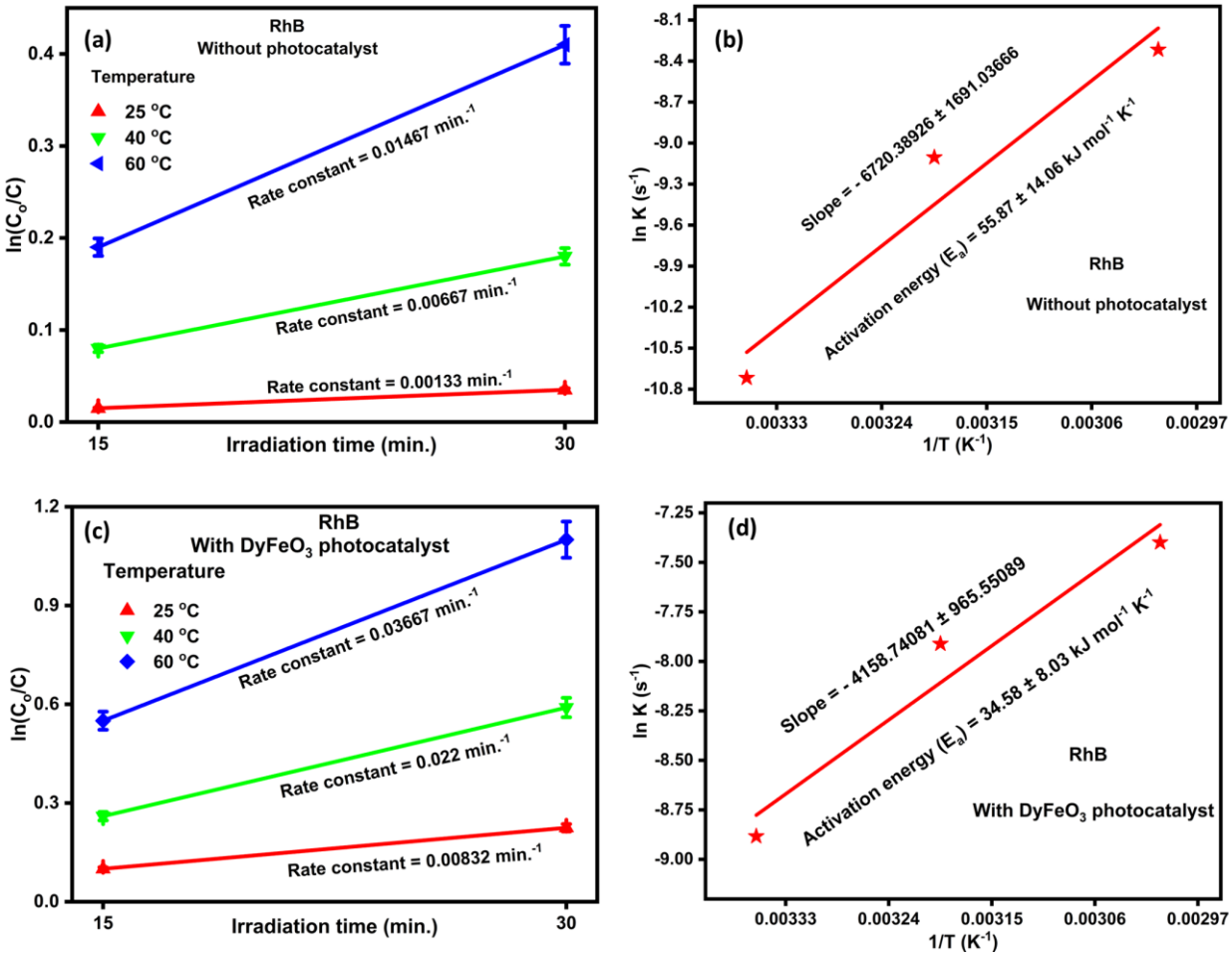

Fig. S7 *Activation energy measurement of RhB. (a,c) Pseudo-first-order kinetics of RhB without and with the presence of $DyFeO_3$ photocatalyst, respectively. (b,d) Arrhenius plot of RhB without and with the presence of $DyFeO_3$ photocatalyst, respectively. $DyFeO_3$ substantially decreased the activation energy of RhB compared to the case of without photocatalyst. These results indicate the true photocatalytic activity of $DyFeO_3$ nanoparticles.*

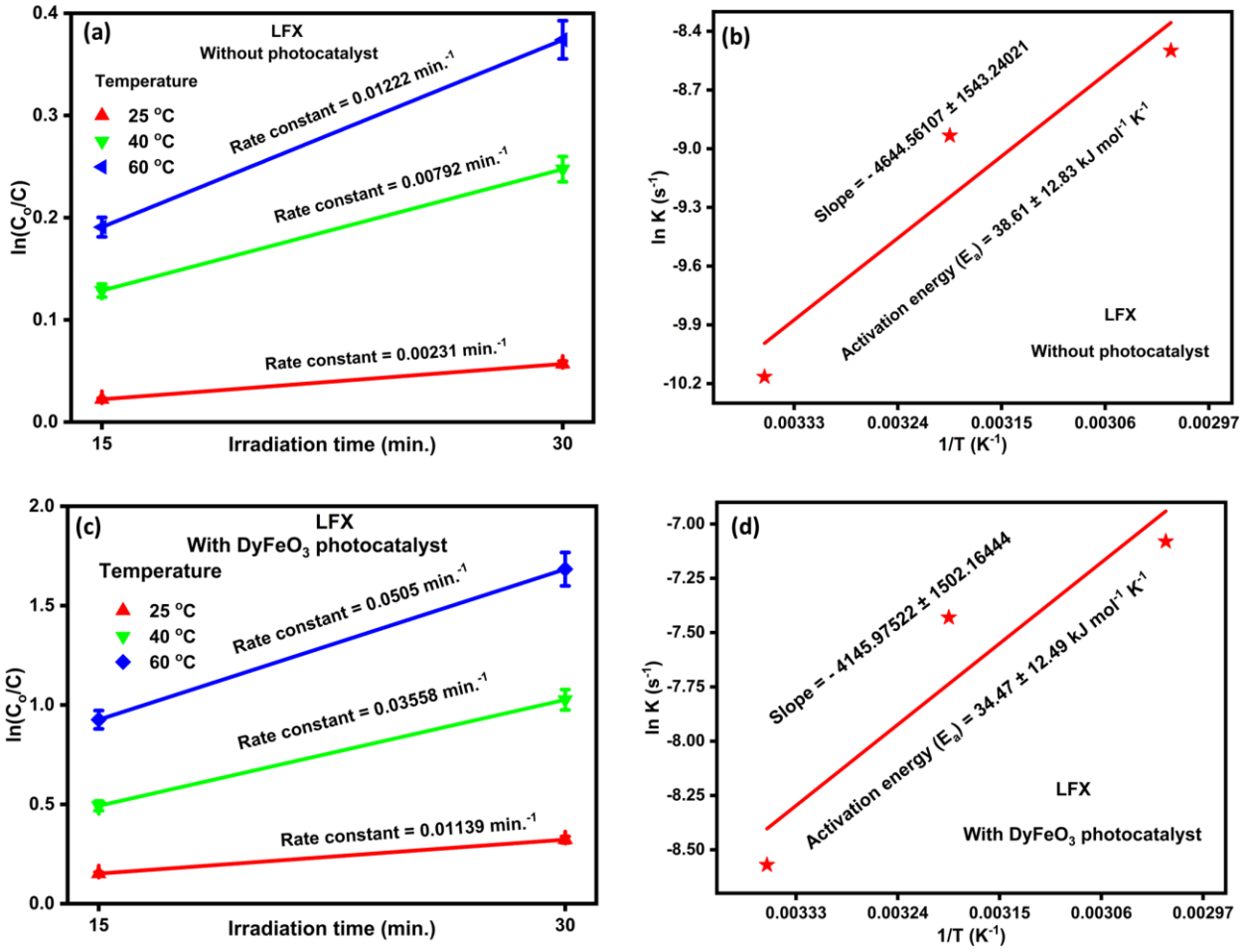

Fig. S8 *Activation energy measurement of LFX. (a,c) Pseudo-first-order kinetics of LFX without and with the presence of $DyFeO_3$ photocatalyst, respectively. (b,d) Arrhenius plot of LFX without and with the presence of $DyFeO_3$ photocatalyst, respectively. $DyFeO_3$ substantially decreased the activation energy of LFX compared to the case of without photocatalyst. These results indicate the true photocatalytic activity of $DyFeO_3$ nanoparticles.*

Apparent Quantum Yield (AQY) calculation

Step 1: Degraded pollutant molecule calculation

Detail	Unit	RhB (DFO)	LFX (DFO)
Pollutant solution	L	0.05	0.05
Pollutant concentration	g/L	0.012	0.01
Pollutant weight in solution	g	0.0006	0.0005
Molecular weight	g/mol	479.02	361.368
No. of moles in a solution	mol	1.25×10^{-6}	1.38×10^{-6}
No. of molecules in a mole	molecules/mol	6.02×10^{23}	6.02×10^{23}
Total no. of pollutant molecules	molecules	7.53×10^{17}	8.31×10^{17}
Degradation percentage	%	85.9	88.38
No. of degraded molecules	molecules	6.47×10^{17}	7.34×10^{17}

Step 2: Photon energy calculation

Wavelength of light λ = 440 nm = 440×10^{-9} m

Energy of one photon $E = \frac{hc}{\lambda} = \frac{6.6\times10^{-34}\times3\times10^{8}}{440\times10-9} = 4.50 \times 10^{-19}\, Joules$

The total energy of light falling per second per unit area is

$$E_{Total} = 100\, mW\, cm^{-2} = 100 \times 10^{-3} \times 10^{4} W\, m^{-2} = 1000\, W\, m^{-2}$$

Number of Photon = $\frac{E_{Total}}{\mathrm{E}} = \frac{1000}{4.50\times10^{-19}} = 2.22 \times 10^{21}$

Area of exposed solution = $\frac{2\pi rl}{2} = \pi rl$

Total number of Photon falling on the solution (Number of incident Photon) = Number of Photon × Area of exposed solution

Apparent Quantum Yield (AQY) = $\frac{Number\ of\ degraded\ molecule}{Number\ of\ incident\ photon} \times 100$

Irradiation time (min.)	Area of exposed solution (m^2)	Number of incident photon	Apparent Quantum Yield (%) in RhB (DFO)	Apparent Quantum Yield (%) in LFX (DFO)
240	0.001007	2.24×10^{18}	28.94	32.83

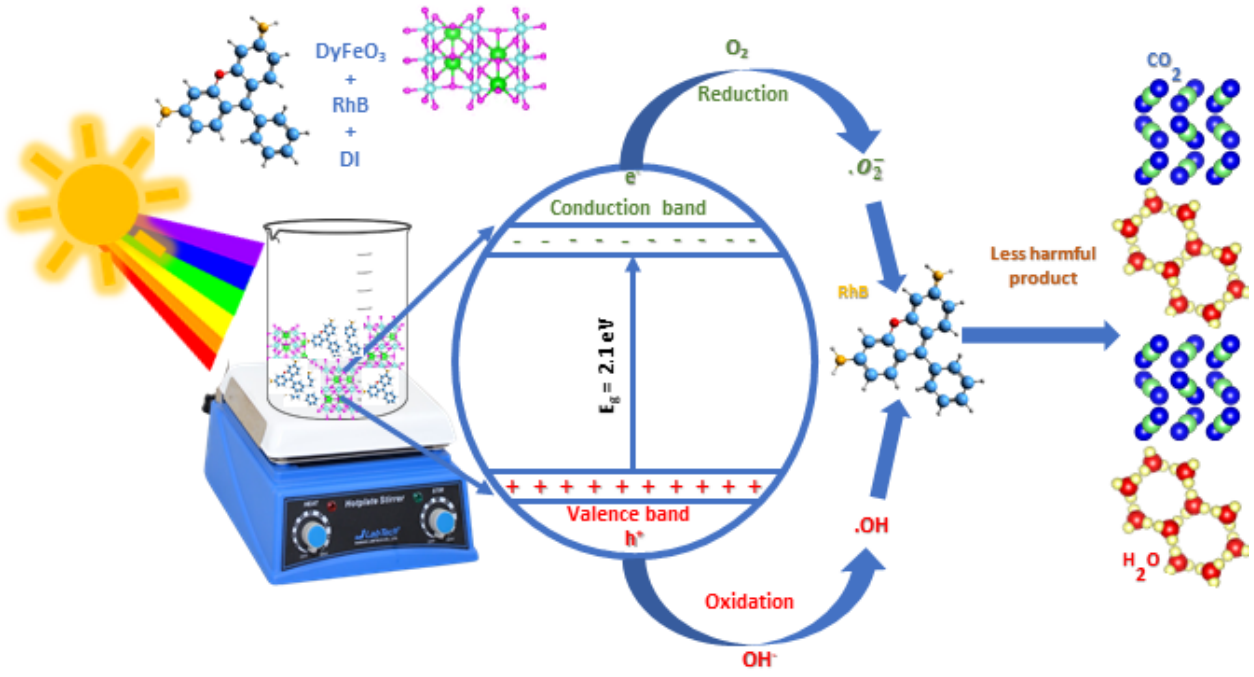

Fig. S9 *Schemetic representation of the RhB degradation mechanism with the presence of $DyFeO_3$ photocatalyst. The proposed pollutant degradation principle by $DyFeO_3$ nanoparticles is schematically depicted. Sunlight absorption by the nanoparticles generates electron-hole pairs, initiating redox reactions with water and oxygen to yield superoxide ($\bullet O_2^-$) and hydroxyl (•OH) free radicals. These radicals facilitate the breakdown of organic pollutants into simpler, less harmful compounds such as H_2O and CO_2.*

References:

1. M. Tarek, F. Yasmeen and M. A. Basith, *ChemRxiv.*, 2024, DOI: 10.26434/chemrxiv–2024–5b3qt–v3
2. N. Joshi, M. N. Romanias, V. Riffault and F. Thevenet, *Aeolian res*., 2017, **27**, 35–45.
3. T. V. Rozario, F. Sharmin, S. Shamim and M. Basith, *Ceram. Int.,* 2024, **50**, 3606–3617.
4. Z. Behzadifard, Z. Shariatinia and M. Jourshabani, *J. Mol. Liq.*, 2018, **262**, 533–548.
5. S. Guan, R. Li, X. Sun, T. Xian and H. Yang, *Mater. Technol.*, 2021, **36**, 603–615.
6. M. N. Ha, L. Wang and Z. Zhao, *Res. Chem. Intermediate*, 2019, **45**, 1493–1508.
7. C. Wang, S. Gao, J. Zhu, X. Xia, M. Wang and Y. Xiong, *J. Environ. Sci.*, 2021, **99**, 249–259.